



# Bipyridine-Proline Grafted Silicas with Different Mesopore Structures: Their Catalytic Performance in Asymmetric Aldol Reaction and Structure Effect

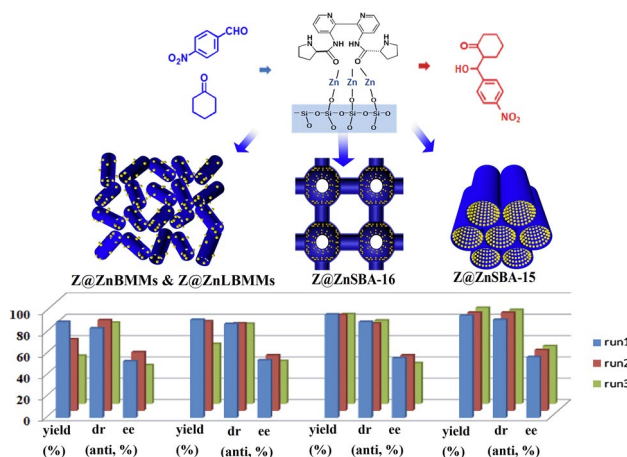
Xu He<sup>1</sup> · Shiyang Bai<sup>1</sup> · Jihong Sun<sup>1</sup> · Yajing Zhang<sup>1</sup> · Hongwu Zhao<sup>1</sup> · Xia Wu<sup>1</sup>

Received: 6 February 2018 / Accepted: 16 May 2018 / Published online: 21 June 2018  
© Springer Science+Business Media, LLC, part of Springer Nature 2018

## Abstract

A series of immobilized bipyridine-proline based on mesoporous silica with different structures were synthesized via grafting followed by coordination method. All catalysts were used in asymmetric aldol reaction of cyclohexanone with 4-nitrobenzaldehyde, and their catalytic performance including activities and stabilities have been investigated. The results indicated that the pore structure, morphology, and even the particle dispersity all showed the effects on the catalytic performance of immobilized catalysts.

## Graphical Abstract



**Keywords** Mesoporous silicas · Different structures · Bipyridine-proline · Heterogeneous catalyst · Aldol reaction

**Electronic supplementary material** The online version of this article (<https://doi.org/10.1007/s10562-018-2421-5>) contains supplementary material, which is available to authorized users.

- ✉ Shiyang Bai  
sybai@bjut.edu.cn
- ✉ Jihong Sun  
jhsun@bjut.edu.cn

<sup>1</sup> Beijing Key Laboratory for Green Catalysis and Separation, Department of Chemistry and Chemical Engineering, Beijing University of Technology, 100 PingLeYuan, Chaoyang District, Beijing 100124, People's Republic of China

## 1 Introduction

The aldol reaction is recognized as being one of the most powerful and popular methods for the construction of C–C bonds. Organocatalysis [1], in particular the amino acid proline [2–4] and its derivatives [5, 6], have been demonstrated to be one of the most potential catalysts in the field of asymmetric aldol condensations. However, the homogeneous catalyst suffers many problems, including difficulty in separation from the reaction mixture and recycling, and moreover the organocatalyst are usually used in a substantial

quantity, in some cases up to 30 mol%. From a practical and environmental point of view, it would be desirable to transfer the catalysts into heterogeneous media, and immobilization is proved to be the simplest method to achieve this heterogeneity. After the immobilization the product purification and the catalyst recycling can be facilitated [7, 8], which is meaningful for the environmental protection and energy conservation, especially when the catalyst is obtained after several synthetic steps.

Various materials (e.g., alumina, mesoporous silica materials, polymers, carbon materials, zeolites) can be used as the supports of immobilized organic catalysts [9–12]. Among these supports, the mesoporous silica materials have received much attention because of their large surface areas, uniform ordered mesoporous channels, high hydrothermal stability, easy functionalized surfaces property and tunable pore dimension and channel structure [13–15]. More importantly, the nanopores of these mesoporous supports can influence the catalytic reaction process [16, 17], resulting in the different catalytic performances. For example, Calderón et al. immobilized L-proline onto mesoporous silica through a direct synthesis method [18]. It was found that the material showed higher enantioselectivity than the homogeneous counterpart in the diethyl malonate addition reaction due to the short channel pore structure of the silica support, and the heterogeneous catalysts could be reused without significant loss of stereoselectivity. Gao et al. [19] functioned the highly ordered 2D hexagonal mesostructure and disordered foam-like mesostructure mesoporous materials with L-prolinamide by using different silicon precursors in HAc–NaAc buffer solution, in the asymmetric aldol reaction of cyclohexanone and 4-nitrobenzaldehyde, the materials with orders mesostructure exhibited higher enantioselectivity (91% ee) than that with disordered foam-like mesostructure (75% ee). Lou et al. [20] demonstrated the influence of the pore architecture and the size of the catalysis loading amount by using MCM-48, SBA-15 and functioned SBA-16 as catalysis support, and pointed out the influences of mesoporous structure type and pore size on the controlled heterogeneous catalysis. Although, some heterogeneous catalysts have achieved comparable activity to the homogeneous ones, in most cases two conflicting problems, activity and stability, perplex the synthesis of immobilized catalysts. In the catalysis process the immobilized organic catalyst must coordinate with the substrates and change configuration, which means that the mobility of the confined catalysts are of great importance to the activity. But on the other hand, to maintain the high stability, the protection of immobilized catalyst by carrier confinement against leaching is necessary. Many works focus on the interaction method and linking group between the organic catalyst and the supports [16, 17]. However, to the best of our knowledge, the intensive research about the synthetic strategy including the effect of different structures

and morphology of mesoporous material have seldom been systemically investigated.

In our previous studies, the bimodal mesoporous SiO<sub>2</sub> (BMMs: bimodal mesopores with small mesopores of around 3 nm and the large mesopores of uniform intra-nanoparticle [21]) were employed as the carrier to immobilize the bipyridine-proline, and the hybrid materials was proved to be efficient in aldol reactions even compared with the homogenous counterpart [22]. But the catalyst was not stable enough to maintain the high activity in the recycling process. Herein, based on our previous work [22], BMMs with different pore size, SBA-16 and SBA-15 supported organocatalysts were prepared using metal Zn acetate as the anchor to graft the bipyridine-proline derivative. As catalysts for the asymmetric aldol reaction of cyclohexanone with 4-nitrobenzaldehyde [23], the catalytic performances were investigated in detail to demonstrate the influences of pore structure and pore size of different supports on the catalytic activities and stability.

## 2 Experimental Section

### 2.1 Chemicals

Cetyltrimethylammonium bromide (CTAB), tetraethyl orthosilicate (TEOS) and 1, 3, 5-trimethylbenzene single component (TMB) were purchased from Sinopharm Chemical Reagent Beijing Co., Ltd. Amorphous SiO<sub>2</sub>, tri-block copolymer poly(ethylene oxide)-poly(propylene oxide)-poly(ethylene oxide) (P123) and polyoxyethylene-polyoxypropylene block copolymer (F127) were purchased from Aldrich. Ammonium hydroxide (25%, NH<sub>3</sub>·H<sub>2</sub>O), absolute methanol, hydrogen nitrate, and Na<sub>2</sub>SO<sub>4</sub> were obtained from Beijing chemical works. The catalyst [(2S,2'S)-N,N'-([2,2'-bipyridine]-3,3'-diyl)bis(pyrrolidine-2-carboxamide)] (Z) (the structure of Z is shown in Illustrate 1) was synthesized according to the previous report [11, 12]. Zinc acetate, dimethyl sulfoxide (DMSO) were purchased from Tianjin Fuchen chemical reagents factory. Dichloromethane was distilled from the appropriate drying agents immediately before use, purified under reduced pressure. All of the solvents and reagents were of analytical reagent grade. Deionized water was used in all experiments.

### 2.2 Characterization

The powder X-ray diffraction (XRD) measurement was carried out with a Bruker-AXS D8 Advance X-ray diffractometer using CuK $\alpha$  radiation (=0.154056 nm) within the scattering angle 2 $\theta$  range of 1°–10°, 10°–50° respectively, and the accelerating voltage was set at 36 kV with a 20 mA flux. The scanning electron microscopy (SEM) images were

undertaken on a Hitachi field-emission scanning electron microscope (S-4300) (accelerating voltage of 5 kV and resolution of 6.6 mm). The transmission electron microscopy (TEM) micrographs were captured on a FEI field emission transmission electron microscope (Tecnai G2 F30) and the accelerating voltage is 300 kV. Samples for TEM measurements were made by casting one drop of the sample's ethanol solution on carbon-coated copper grids. The Fourier transform infrared spectroscopy (FT-IR) spectra were measured recorded on a Nicolet 6700 spectrometer using a KBr pellet technique. The spectral resolution was 4 cm<sup>-1</sup>, and 32 scans were recorded for each spectrum. The thermogravimetric analysis (TGA) measurements were carried out on a Perkin-Elmer Pyris 1 TG instrument from 25 to 800 °C at a heating rate of 10 °C/min under the N<sub>2</sub> atmosphere with a flow rate of 20 mL/min. The sample (mass of around 3 mg) was heated in a standard platinum sample pan. The N<sub>2</sub> adsorption/desorption isotherms were measured at -196 °C on a Micromeritics Tristar II 3020 analyzer. All samples were previously outgassed at 80 °C for 6 h before measurements. Specific surface areas of each material were calculated by Brunauer-Emmett-Teller (BET) model, the plots of the corresponding pore size distribution was evaluated from desorption branches with the model of Barrett-Joyner-Halenda (BJH). The total pore volumes were estimated from the amounts adsorbed at a relative  $P/P_0$  of 0.99. The UV-vis DR spectra were carried out in the wavelength range of 200–800 nm with a Shimadzu UV-2600 spectrophotometer. The metal content was tested by PerkinElmer Optima 7000DC inductively coupled plasma optical emission spectrometer (ICP). <sup>13</sup>C NMR spectra was recorded at 300 and 75 MHz, respectively, using a Varian Mercury Vx-300 spectrometer. The enantiomeric excesses were determined by HPLC analyses on a Waters system equipped with a photodiode array detector (monitoring at 200–400 nm), using Chiracel AD and AS-H column (25 cm × 0.46 cm) by Daicel Chemical Ind., Ltd.

### 2.3 Synthesis of Mesoporous Silicas

The synthesis procedure of BMMs was partially similar to the method reported by Sun et al. [23]. The synthesis procedure of BMMs with larger mesopores was based on the method reported by Sun et al. [24], and used TMB as a silica source to expand the pore size [25], and the molar composition was as follows: 0.206 CTAB: 1 TEOS: 1.2 NH<sub>4</sub>OH: 165.55 H<sub>2</sub>O: 0.946 TMB. The main synthesis procedure was almost the same as BMMs except that TMB was added into the system together with TEOS. The resulting sample was denoted as LBMMs.

SBA-15 materials were prepared according to the procedure reported by Coppens et al. [26] using P123 as a structure-directing agent and TEOS as silica source.

SBA-16 materials were prepared according to the procedure reported by Rosen [27] using P123 and its mixtures with F127 as a structure-directing agent and TEOS as silica source.

### 2.4 Preparation of Zn Functionalized Mesoporous Silicas

0.5 g calcined mesoporous silicas (BMMs, LBMMs, SBA-15, SBA-16) was treated at 120 °C under vacuum for 3 h to remove physical absorbed water in a round-bottom flask and allowed to cool to room temperature under N<sub>2</sub> atmosphere. Then, 50 mL of Zn(OAc)<sub>2</sub>·4H<sub>2</sub>O solution of dried methanol with mole ratio of 50% was added into the flask, after stirring for 10 h at room temperature, the mixture was collected by rotary evaporation, and dried for 8 h at 60 °C. In order to remove excess zinc acetate, the powder was washed several times using deionized water, methanol and then dried overnight. Thus, the sample was denoted as ZnBMMs, ZnLBMMs, ZnSBA-16 and ZnSBA-15. The contents of the Zn in Zn functionalized mesoporous silicas are presented in Table S1 tested by ICP.

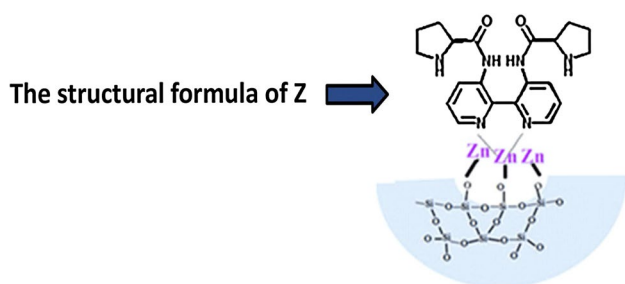
### 2.5 Preparation of Bipyridine-Proline-Immobilized Mesoporous Silica Catalysts

Taking ZnBMMs as an example, 0.1092 g Z was dissolved in 2 mL dried dichloromethane and added into the flask which already contained 0.3 g Zn functionalized mesoporous silicas (the additive amount was based on the proportion of n (Z) and n (Zn) around 1:1, the content of Zn in Zn functionalized mesoporous silicas are presented in Table S1). After refluxing for 12 h, the obtained solid was thoroughly washed by DMSO and CH<sub>2</sub>Cl<sub>2</sub> alternately for 48 h, in which, the used solvent was replaced every two hours to remove the remaining non-supported Z (confirm by UV-vis spectrum). The obtained product was dried at 40 °C under vacuum, which was designated as Z@ZnBMMs. Z@ZnLBMMs, Z@ZnSBA-16 and Z@ZnSBA-15 were prepared using the same method.

### 2.6 Catalytic Reactions

The typical procedure for the direct asymmetric aldol reaction was as follows: desired amount of solid catalyst (containing 0.02 mmol of Z) were added to a suspension of cyclohexanone (0.1 mmol), solvent (water, 0.5 mL) and trifluoroacetic acid (0.2 μL). The mixture was stirred for 5 min followed by the addition of 4-nitrobenzaldehyde (0.1 mmol). The resulting mixture was stirred at room temperature. Reactions were monitored by TLC carried out on 0.25 mm SDS silica gel coated glass plates (60F254) and compounds were detected with UV light. After dried with

anhydrous  $\text{Na}_2\text{SO}_4$ , the reaction mixture was purified by flash chromatography on silica gel (eluent: EtOAc / petroleum ether) to give a mixture of syn-aldol and anti-aldol products. The dr (diastereomeric ratio) value and ee% value are determined by chiral HPLC analysis. Compared with reported chiral HPLC analysis data, the absolute configuration of the major anti product is (1'R, 2S). After filtration, the catalyst was separated and washed thoroughly with dichloromethane. The catalyst could be directly used for the next run after drying under vacuum (Scheme 1).



**Scheme 1** Illustration of the bipyridine-proline functionalized mesoporous materials

## 3 Result and Discussion

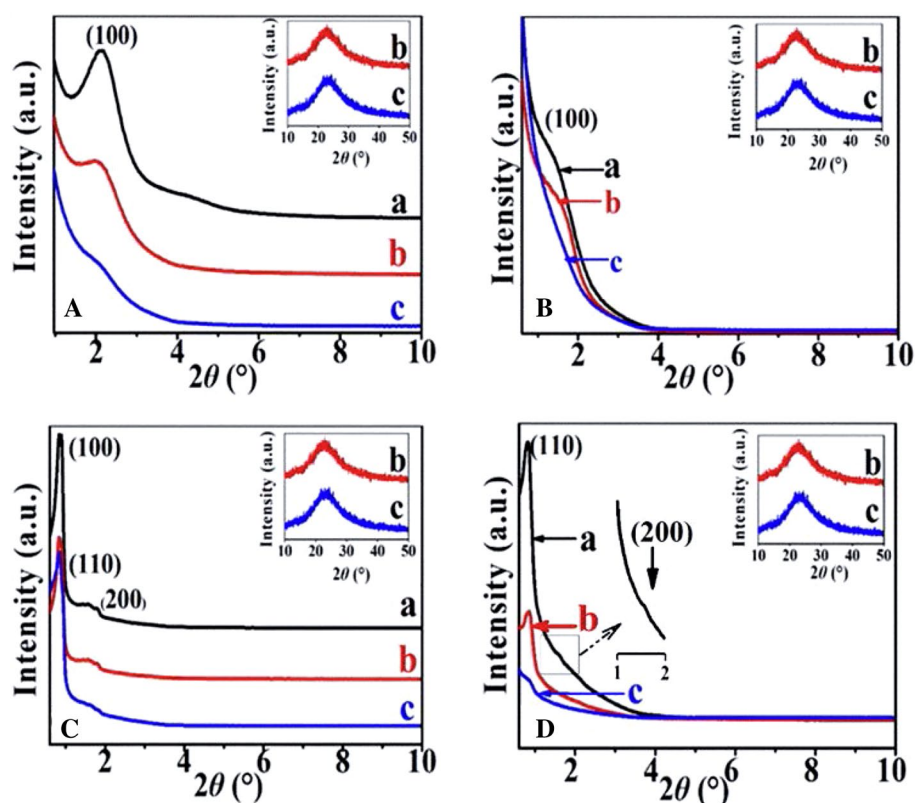
### 3.1 Structure Characterizations

#### 3.1.1 XRD Patterns

The representative XRD patterns of BMMs, LBMMs, SBA-15, SBA-16 series samples are presented in Fig. 1. As can be seen, the XRD pattern of BMMs (Fig. 1A-a) and LBMMs (Fig. 1B-a) clearly exhibited one reflection in the  $2\theta$  range of  $2^\circ$ – $10^\circ$ , indexed as (100) peak, which can be associated with the existence of the mesoporous structure [24]. Three characteristic reflection, (100), (110) and (200) peaks were observed in SBA-15 (Fig. 1C-a), indicating the order hexagonal mesoporous structure [28]. For SBA-16 (Fig. 1D-a), two characteristic reflections, (110) and (200) peaks were observed, which can be associated with the existence of the cubic  $Im\bar{3}m$  mesoporous structure [9].

After grafting with  $\text{Zn}(\text{OAc})_2 \cdot 2\text{H}_2\text{O}$  into the mesoporous surfaces, the peak intensity all decreased and their position ( $2\theta$ ) shifted to the larger angles, implying the  $d$  space was shrunken and the successful introduction of functional groups onto the mesoporous surface [29]. Particularly, after Z loading, more broaden reflection peaks with decreased peak intensity for samples (Fig. 1A–D-c) were detected suggesting that the ordered mesoporous framework was still

**Fig. 1** XRD patterns of **A** BMMs, **B** LBMMs, **C** SBA-15, **D** SBA-16 series samples. *a* pure mesoporous materials, *b* samples after grafting metal zinc, *c* samples immobilized Z





maintained but disturbed by the grafting of Z. Meanwhile, the results further revealed the successful introduction of the Z in mesoporous channels of modified mesoporous silica. On the other hand, there was only one peak around  $2\theta$  of  $20^\circ$ – $30^\circ$  in the wide angle XRD patterns for all of the samples, indicating the inexistence of ZnO.

### 3.1.2 $N_2$ Adsorption and Desorption Isotherms

Figure 2 presents the  $N_2$  adsorption/desorption isotherms and corresponding pore size distributions (inset) of BMMs (Fig. 2A), LBMMs (Fig. 2B), SBA-15 (Fig. 2C) and SBA-16 (Fig. 2D) series samples, two well-defined sharp inflections observed in  $p/p_0$  ranges 0.3–0.6 and 0.8–1.0 for BMMs (Fig. 2A-a) and LBMMs (Fig. 2B-a), verifying the existence of bimodal mesopores with a narrow small pore distribution around 2.6–4.0 nm and a large pore distribution around 20–30 nm, which is originated from the accumulation of the intra-spherical particles [24, 28]. The isotherm pattern of SBA-15 (Fig. 2C-a) is typical type IV adsorption isotherm and H1 type hysteresis loop, characteristic of highly ordered 2D hexagonal mesostructured. The SBA-16 (Fig. 2D-a) shows type IV adsorption isotherm and H2 type hysteresis loop, which is typical of mesoporous material with cage-like pore structure. However, compared with BMMs and LBMMs, the pore size distributions of SBA-15 (inset Fig. 2C) and SBA-16 (inset Fig. 2D) presented only one pore distribution around 6.94 and 4.15 nm respectively, verifying the different mesoporous geometry between BMMs and LBMMs. Moreover, all the samples maintain the same isotherms shape compared with their original supports after the modifying of Zn and further grafting of Z. This

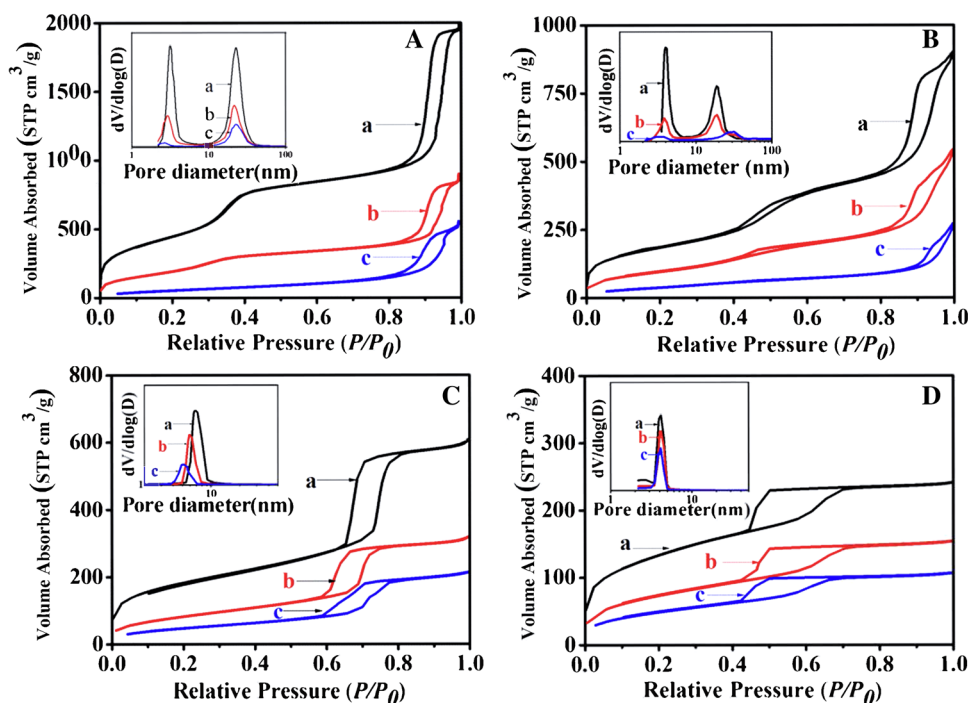
indicated that the structure of the support was maintained in the process of the immobilization of Z.

The textural parameters of various materials calculated by  $N_2$  adsorption–desorption isotherms are presented in Table S1. Compared with parent supports, the metal-modified samples ZnBMMs, ZnLBMMs, ZnSBA-15 and ZnSBA-16 exhibited decreased BET surface area, pore volume, and pore size. This indicates that the metal groups are located mainly on the inner surfaces of samples. After immobilization of Z, a further decrease in BET surface area, pore volume, and pore size was observed, suggesting that Z is present inside the channels of modified materials. Along with the result of XRD, this is a strong evidence to prove the successful immobilization of Z.

### 3.1.2 SEM and TEM Micrographs

The SEM images, depicted in Fig. 3A, clearly demonstrated that the BMMs (Fig. 3A-a) and LBMMs (Fig. 3A-b) possessed nanosized spherical particles, and the corresponding size distribution was around less than 50 nm. At the same time, LBMMs was more evenly divided than BMMs. However, different from BMMs and LBMMs consisted of irregular bulk powder in Fig. 3A-a, A-b, SBA-15 (Fig. 3A-c) presented the bamboo-like morphology, SBA-16 (Fig. 3A-d) presented the uniform sphere morphology. Besides, TEM image for BMMs (Fig. 3B-a) further confirmed the presence of spherical particles with a large number of narrow small pores around 3 nm. While, according to the TEM image of SBA-15 (Fig. 3B-c) and SBA-16 (Fig. 3B-d),

**Fig. 2**  $N_2$  adsorption/desorption isotherms and corresponding pore size distributions (inset) of **A** BMMs, **B** LBMMs, **C** SBA-15, **D** SBA-16 series samples. *a* pure mesoporous materials, *b* samples after grafting metal zinc, *c* samples with immobilized Z



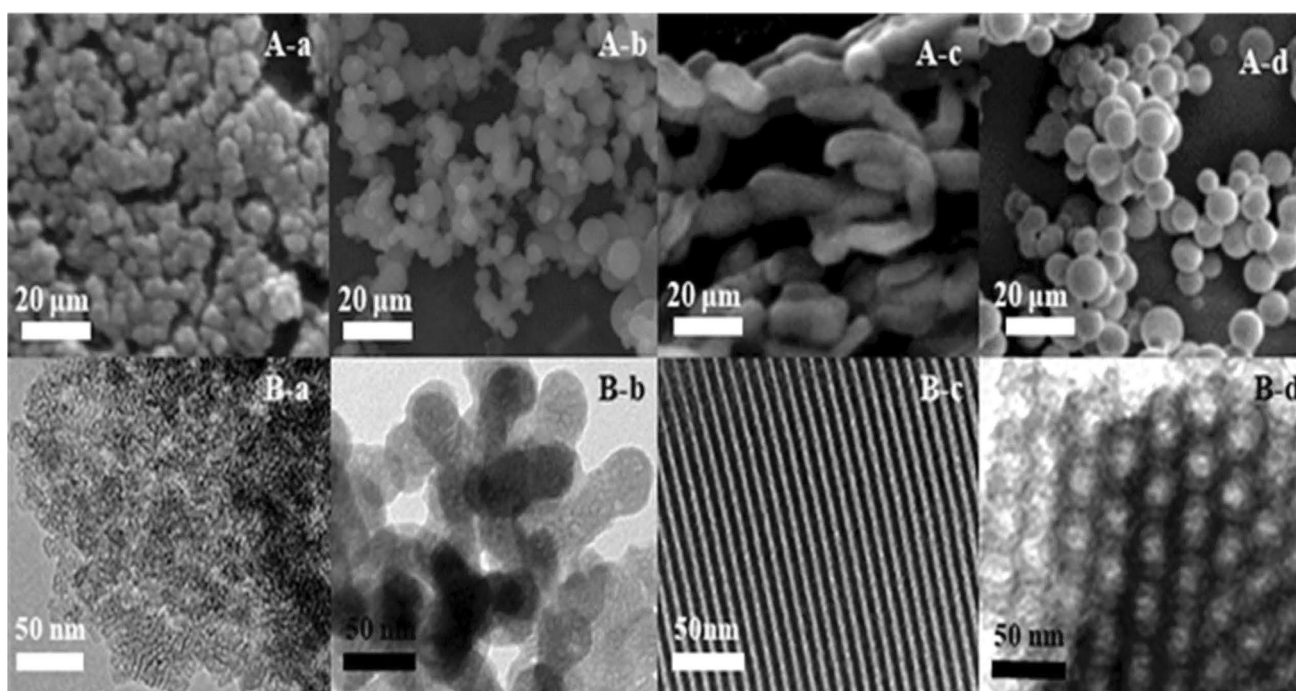


**Fig. 3** SEM **A** and TEM **B** images of *a* BMMs, *b* LBMMs, *c* SBA-15, and *d* SBA-16

only well-order mesopores about 7 and 4 nm were observed respectively. It is obvious that BMMs, LBMMs and SBA-16 both possessed small mesopores around 3–4 nm, but due to the different morphology, the 3–4 nm mesopores channels of BMMs and LBMMs were short and random, while SBA-16 showed long and order three-dimensional mesoporous structures [21, 24]. Meanwhile, the particle size and the mesopore size of SBA-15 were much larger than that of BMMs, LBMMs and SBA-16.

## 3.2 Compositional Information

### 3.2.1 UV-Vis DR Spectra

The UV-visible diffuse reflectance spectra of samples including before and after grafting Z were recorded in the range of 200–800 nm and the spectral traces are provided in Fig. 4. Taking SBA-15 series as examples, as can be seen, the UV adsorption peaks of Z@ZnSBA-15 (Fig. 4c), and Z (Fig. 4d) in the range of 250–350 nm were corresponding to  $\pi \rightarrow \pi^*$  and  $n \rightarrow \pi^*$  transitions of Z [30]. In contrast, there was no absorption peak for SBA-15 (Fig. 4a) and ZnSBA-15 (Fig. 4b) in the range of 200–600 nm. Therefore, it can be easily deduced that the Z was successfully incorporated onto the surface of the SBA-15. The other three kinds of catalysts, such as Z@ZnBMMs, Z@ZnLBMMs and Z@ZnSBA-16, showed the similar results. This is a direct proof of Z introduction

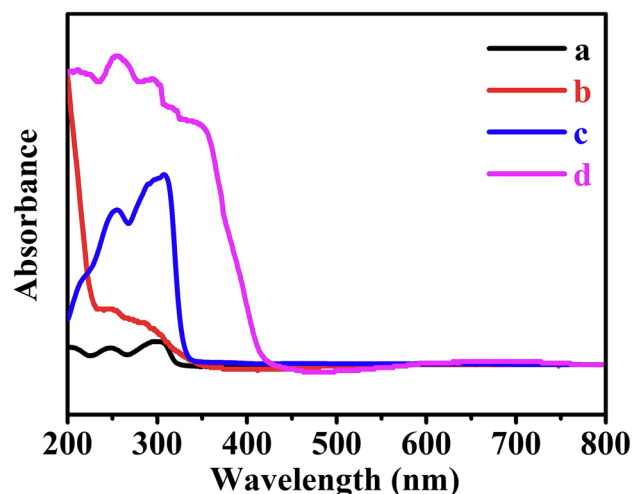


**Fig. 4** UV-vis DR spectra of SBA-15 series *a* pure mesoporous material, *b* sample after grafting metal zinc, *c* sample with immobilized Z, and *d* Z

into the channel of ZnBMMs, ZnLBMMs, ZnSBA-15 and ZnSBA-16. FT-IR was also employed as the composition characterization (Fig. S1) and the FT-IR spectrum of all the catalysts showed that the typical absorption bands in the region of  $1600\text{--}1300\text{ nm}^{-1}$  belonged to stretching vibrations of pyridine rings and C=O stretching vibrations of Z, which clearly indicates that Z was incorporated into the solid supports [31].

### 3.2.2 $^{13}\text{C}$ NMR Spectra

The  $^{13}\text{C}$  NMR spectra of SBA-15, and Z@ZnSBA-15 are shown in Fig. 5. Z@ZnSBA-15 as shown in Fig. 5a presented few characteristic peaks, in which, the three peaks observed at 28.85 ppm, 33.48 and 47.38 ppm were assigned to the pyrrolidine carbons of Z, and these characteristic peaks were found in similarity with the literature [32, 33]. Comparably, all characteristic peaks were not found in the spectra of SBA-15 (Fig. 5b), which confirms the absence of organic functional groups. Therefore, these results indicated that the Z molecules were successfully modified on the surface of Zn-grafted sample.

### 3.3 Catalytic Properties of Different Kinds of Mesoporous Immobilized Catalysts

The heterogeneous catalysts, Z@ZnBMMs, Z@ZnLBMMs, Z@ZnSBA-15 and Z@ZnSBA-16 were evaluated in the aldol reaction of cyclohexanone and 4-nitrobenzaldehyde at room temperature using water as solvent and trifluoroacetic acid as promotor. As can be seen in Fig. 6 and Table 1, to attain the yield of more than 90%, 5 days were taken for Z@ZnBMMs and Z@ZnLBMMs which were a bit lower than that of the homogeneous one, but for Z@ZnSBA-16 (4 days, 96%) and Z@ZnSBA-15 (2 days, 97%), higher activity than the homogeneous one was achieved. However, the enantioselectivities of heterogeneous catalysts were lower than that of homogeneous one. Although, the ee values of all catalysts are lower than that of homogeneous one, their dr values, such as Z@ZnBMMs (84:16), Z@ZnLBMMs (88:12), Z@ZnSBA-16 (90:10), and Z@ZnSBA-15 (92:8), were a little bit lower than that of homogeneous one (95:5) but comparable. Compared with the homogeneous Z, the unsatisfactory

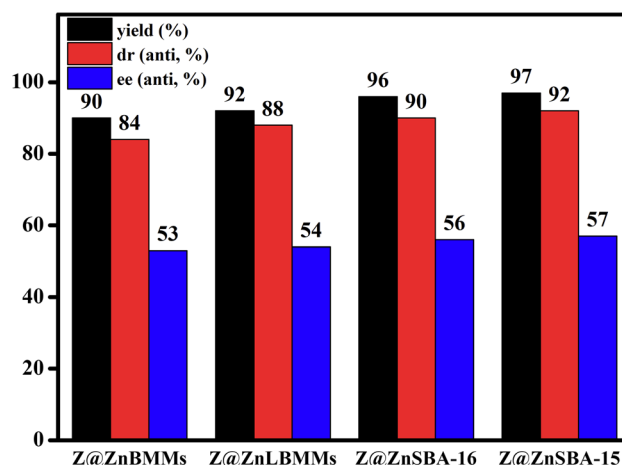
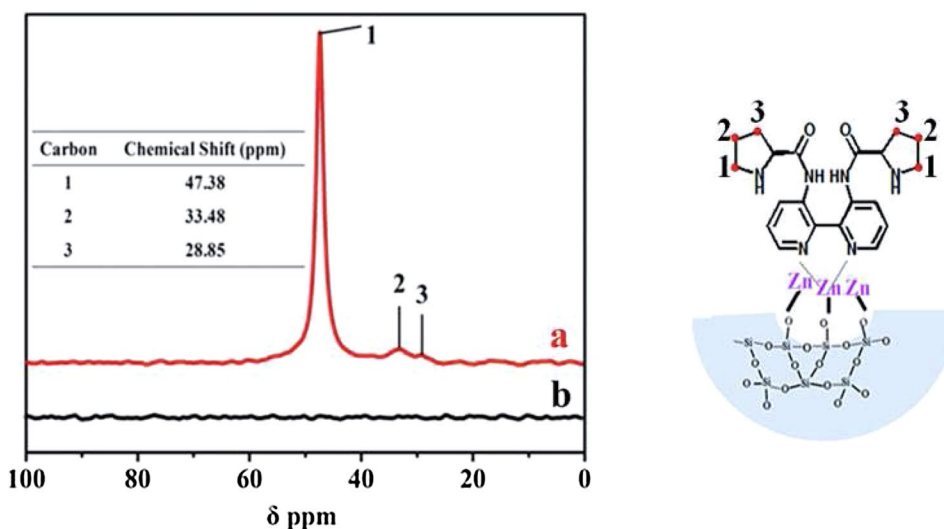
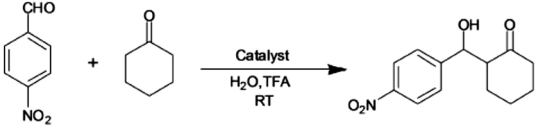


Fig. 6 The reaction results of catalysts Z@ZnBMMs, Z@ZnLBMMs, Z@ZnSBA-16 and Z@ZnSBA-15 in the aldol reaction

enantioselectivities were mainly due to the mesopore confinement, which limit the free configuration change of Z and substrates [20]. In short, the catalytic activity and enantioselectivity of these catalysts decreased as the order of Z@ZnSBA-15 > Z@ZnSBA-16 > Z@ZnLBMMs > Z@ZnBMMs, which was also the order of the pore size of the solid supports. In other words, the synthesized heterogeneous catalysts with the largest pore size presented the highest catalytic activity, no matter what the channel structure was. This phenomenon could be explained as that: in the aldol reaction of cyclohexanone with 4-nitrobenzaldehyde, both the substrates and products had the large molecular size. When they were activated by the organic catalysts through coordination in the channel, the pore size would restrict their movement and configuration change, and further affect the activity and enantioselectivity.

Fig. 5  $^{13}\text{C}$  solid-state NMR spectra of a Z@ZnSBA-15, b SBA-15, and scheme of corresponding position of carbon (right panel) (The inset Table represents chemical shift of corresponding carbon)



**Table 1** Asymmetric aldol reaction results<sup>a</sup>


Run	Catalyst <sup>a,b</sup>	Time (days)	Yield (%) <sup>c</sup>	dr (anti/syn) <sup>d</sup>	ee (%; anti) <sup>e</sup>
1	Z@ZnBMMs	5	90	84:16	53
	Z@LZnBMMs	5	92	88:12	54
	Z@ZnSBA-16	4	96	90:10	56
	Z@ZnSBA-15	2	97	92:8	57
	Z@ZnSiO <sub>2</sub>	5	60	95:5	63
2	Z@ZnBMMs	5	67	85:15	55
	Z@LZnBMMs	5	84	81:18	52
	Z@ZnSBA-16	5	90	82:18	52
	Z@ZnSBA-15	3	92	92:8	57
	Z@ZnSiO <sub>2</sub>	5	Trace	Trace	Trace
3	Z@ZnBMMs	5	45	76:24	36
	Z@LZnBMMs	5	56	75:25	40
	Z@ZnSBA-16	5	84	78:22	38
	Z@ZnSBA-15	4	90	88:12	54
1	Z <sup>f</sup>	4	89	95:5	85

Reaction conditions: catalysts, cyclohexanone (104 mL), 4-nitrobenzaldehyde (0.1 mmol), solvent (water, 0.5 mL), promotor (trifluoroacetic acid, 0.2 mL), room temperature. The reaction illustration was as follows that:

<sup>a</sup>S/C = 20

<sup>b</sup>Catalyst dosage was calculated according to the result of TG (Fig. S2)

<sup>c</sup>Isolated yield after separation by silica gel

<sup>d</sup>Determined by HPLC

<sup>e</sup>With (2*S*, 1'*R*) configuration

<sup>f</sup>Homogeneous reaction using Z as catalyst [32]

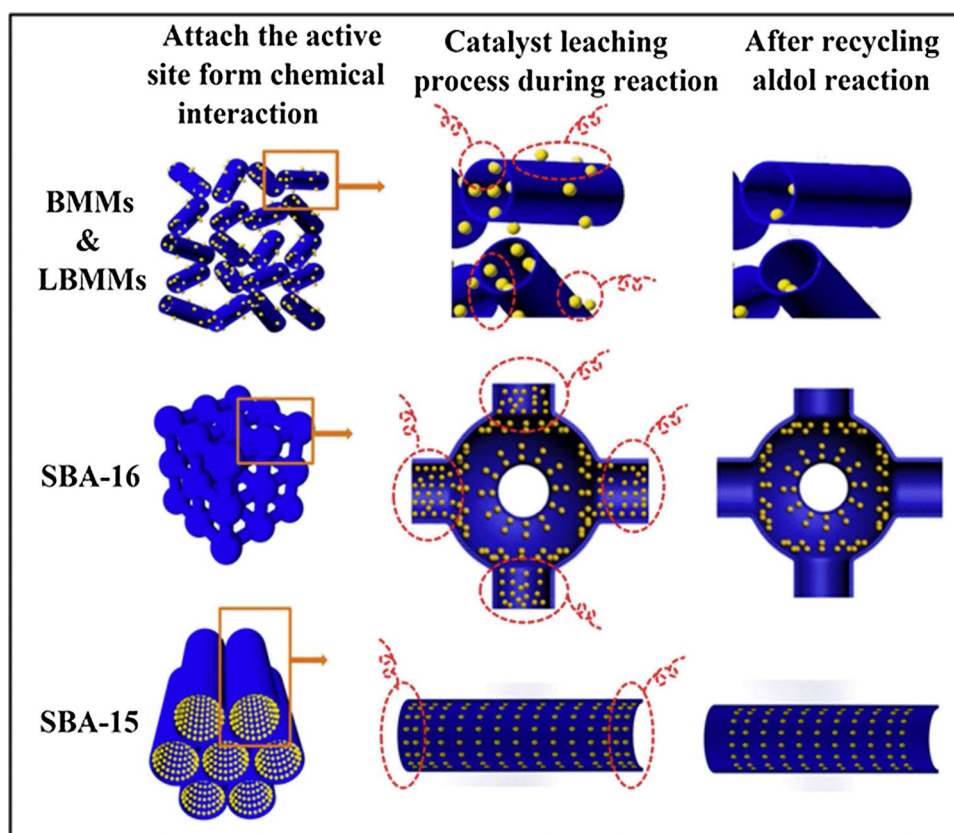
The recyclability is an important indicator for the stability of the immobilized catalysts. The solid catalyst can be easily recovered by filtration with successive washing with dichloromethane and acetone. Table 1 illustrates the recyclability results of all the heterogeneous catalysts for the aldol reaction. According to these results, during the second run, Z@ZnSBA-15 and Z@ZnSBA-16 gave a comparable yield, dr and ee to the first run. Differently, a downward trend was shown in catalytic activity and enantioselectivity in Z@ZnBMMs and Z@ZnLBMMs. However, after the third run, a slight decrease in catalytic reactivity and enantioselectivity was observed in Z@ZnSBA-16, and a significant decrease in catalytic activity and enantioselectivity was observed in Z@ZnBMMs and Z@ZnLBMMs. Nevertheless, Z@ZnSBA-15 was observed maintaining > 90% yield and almost the same enantioselectivity after the third times recycle. However, the activity of SBA-15 still got a little lower based on the fact

that it takes longer time during the reaction with the increase of cycle number. Even so, in the third run Z@ZnSBA-15 also presented the same yield as the homogeneous catalysts. Among the four immobilized catalysts, the SBA-15 based catalyst showed the highest catalytic activity and the best stability for aldol reaction.

Based on the above catalytic results, the possible loading and leaching mechanisms are shown in Scheme 2 pictorially. As stated above, LBMMs showed a little bit better catalytic performance than BMMs in all aspects such as comparable yield, dr and ee value, but not obvious. Compared with BMMs, whose small pore diameter was around 3.14 nm, LBMMs with nano-sized spherical morphology and bigger mesopores whose pore diameter was around 4.02 nm would be beneficial for the catalyst loading and the reactants and products diffusion. Furthermore, in Z@ZnLBMMs less Z was grafted on the secondary pore than BMMs, because



**Scheme 2** Schematic illustration of catalyst loading and leaching process in different mesoporous materials



of the better dispersity of LBMMs than BMMs. And Z in the secondary pore would suffer more exposure to solutions which lead to a more leaching amount of Z during the aldol reaction, so Z@ZnLBMMs showed a little bit better catalyst stability than Z@ZnBMMs. But the influence is not significant. Therefore, the influence of pore diameter and particle dispersity on the stability of the catalyst is not dominant. For BMMs and LBMMs with disorderly nano-sized spherical morphology, the short and two-dimensional mesopores would lead to organic catalysts leaching easily during the reaction process. While, SBA-16, with uniform spherical morphology and the cubic bottle-like mesopores structure whose average pore diameter was 4.15 nm, would be beneficial for catalysts loading, but a large number of Z would be grafted onto the mesopore entrance rather than inside the bottle-like pore channel center. However, Z grafting nearby the pore entrance was more likely to leach into solution than that inside the pore center during the process of reaction. As shown in Scheme 2, compared with BMMs or SBA-16, SBA-15 has longer straight channels with larger pore size (around 6.8 nm), which would cause more Zn and Z be grafted into the middle of the channel and result in better stability. To further prove the importance of the pore confinement, the amorphous SiO<sub>2</sub> was employed as the support to immobilize Z. Although, the higher ee and dr value in the first run was presented by Z@ZnSiO<sub>2</sub>, its yield was

around 60%, much lower than that of other catalysts. After that, the reused Z@ZnSiO<sub>2</sub> presented no any activity. These phenomena may be due to the low surface area and nonporous structures of the amorphous SiO<sub>2</sub>, which resulted in the loading of Z on the outer surface of SiO<sub>2</sub>: on the one hand, the outer surface-loaded Z has the same movement space as the homogeneous system, obvious leading to similar enantioselectivity to homogeneous one. On the other hand, the loaded Z on the outer surface cannot enjoy the protection and confinement of nanopores, easy generating the leaching during the reaction periods. Therefore, catalyst derived from SBA-15 shows the best catalytic performance and stability

**Table 2** The content of Z in catalyst before and after reaction

Catalyst	Content of Z in fresh catalyst (%) <sup>a</sup>	Content of Z in catalyst after recycling (%) <sup>a</sup>	The rate of Z's leaching (%) <sup>b</sup>
Z@ZnBMMs	6	1	83
Z@ZnLBMMs	8	3	63
Z@ZnSBA-16	15	11	27
Z@ZnSBA-15	18	15	17

<sup>a</sup>Content of Z in fresh catalyst and catalyst after recycling was calculated according to the result of TG (Fig. S2)

<sup>b</sup>The rate of Z's leaching = Content of Z in fresh catalyst - Content of Z in catalyst after recycling / Content of Z in fresh catalyst

among BMMs, LBMMs, SBA-16 and SBA-15 due to its special channel structure. The content of Z in the solid catalysts before and after the recycling reaction were characterized by TG analysis (Table 2 and Fig. S2) to prove the mechanism deduced. It is encouraging to find that after the third cycle the leaching rates of Z in the heterogeneous catalysts were just following the opposite order to the stabilities:  $Z@ZnSBA-15 < Z@ZnSBA-16 < Z@ZnLBMMs < Z@ZnBMMs$ .  $Z@ZnBMMs$  presented the greatest leaching rate of about 83% which was nearly 5 times more than that of  $Zn@ZnSBA-15$  (17%). The results further confirmed the influences of the mesopore structure and particle morphology of the supports on the catalytic performance proposed above.

## 4 Conclusion

In summary, a new series of hybrid heterogeneous catalyst based on bipyridine-proline as active sites and mesoporous silica with different pore structure, including BMMs, LBMMs, SBA-15 and SBA-16, as solid support were successfully prepared through grafting, as well as applied to the asymmetric aldol reaction. All the heterogeneous catalysts showed the comparable or even better catalytic performance to the homogeneous one. Particularly, the recycle of solid heterogeneous catalyst could be simply achieved by centrifugation and washing. However, catalyst with different structure showed different catalytic performance.  $Z@ZnSBA-15$  was observed the best catalytic activity and stability in the recycle process compared to the other three catalysts, because of its long and large mesoporous channel which provide enough space for the much larger molecules catalysis reaction and protect the organic catalyst against leaching. This study offered us an innovative strategy that to immobilizing the organic catalyst through weak interaction with the carrier, high performance and good stability could be expected by encapsulating the homogeneous catalysts in the solid nano-materials with long channel and large pore size.

**Acknowledgements** This project was supported by the National Natural Science Foundation of China (21576005, 21403011), and the Beijing Municipal Natural Science Foundation (2152005, 2172004).

## References

1. Bayston DJ, Travers CB, Polywka MEC (1998) *Chem Inform* 29:2015–2018
2. Sandee AJ, Petra DG, Reek JN, Kamer PC (2001) *Chem Eur J* 7:1202–1208
3. Jiang D, Gao J, Li J, Yang Q (2008) *Microporous Mesoporous Mater* 113:385–392
4. Davis ME (2002) *Chem Inform* 33:813–821
5. Tang Z, Jiang F, Cui X, Gong LZ (2004) *Proc Natl Acad Sci USA* 101:5755–5760
6. Lou LL, Yu K, Ding F, Peng X (2007) *J Catal* 249:102–110
7. Wang S (2009) *Microporous Mesoporous Mater* 117:1–9
8. López T, Ortiz E, Meza D, Basaldella E (2011) *Mater Chem Phys* 126:922–929
9. Xue X, Li F (2008) *Microporous Mesoporous Mater* 116:116–122
10. Dominguez F, Sabater MJ (2004) *J Catal* 228:92–99
11. Avelino C (2004) *Catal Rev* 46:369–417
12. Heitbaum M, Glorius F, Escher I (2006) *Angew Chem Int Ed* 37:4732–4762
13. Cozzi F (2006) *Adv Synth Catal* 348:1367–1390
14. Thomas JM, Raja R, Lewis DW (2005) *Angew Chem Int Ed* 44:6456–6482
15. Hu Y, Wu P, Yin Y, Zhang H (2012) *Appl Catal B Environ* 111–112:208–217
16. Memorn P, Hutchings GJ (2004) *Chem Soc Rev* 33:108–122
17. Song CE, Lee SG (2002) *Chem Rev* 102:3495–3524
18. Calderón F, Fernández R, Sánchez F (2005) *Adv Synth Catal* 347:1395–1403
19. Gao J, Liu J, Tang J, Jiang D (2010) *Chem Eur J* 16:7852–7858
20. Lou LL, Yu Y, Yu K, Jiang S (2009) *Sci China* 52:1417–1422
21. Sun J, Shan Z, Thomas Maschmeyer A, Coppens MO (2003) *Langmuir* 19:8395–8402
22. Tang Z, Sun J, Zhao H, Bai S (2017) *Microporous Mesoporous Mater* 260:245–252
23. Wu H, Zhang S, Zhang J, Liu G (2011) *Adv Funct Mater* 21:1850–1862
24. Sun J, Shan Z, Maschmeyer T, Moulijn JA (2001) *Chem Commun* 24:2670–2671
25. Zhao D, Feng J, Huo Q, Melosh N (1998) *Science* 279:548–552
26. Pitchumani R, Li W, Coppens MO (2005) *Catal Today* 105:618–622
27. Rosen R (2004) *J Phys Chem B* 108:11480–11489
28. Zhang W, Lu X, Xiu J, Hua Z (2004) *Adv Funct Mater* 14:544–552
29. Gao L, Sun J, Li Y, Zhang L (2011) *J Nanosci Nanotechnol* 11:6690–6697
30. Kitagawa S, Kitaura R, Noro S (2004) *Angew Chem Int Ed* 35(29):2334–2375
31. Chen J, Fang X, Duan X, Ye L (2013) *Green Chem* 16:294–302
32. Zhao HW, Li HL (2012) *Synlett* 23:1990–1994
33. Zhao HW, Yue YY (2012) *Synlett* 31:485–493